



Physicochemical properties and cytocompatibility assessment of non-degradable scaffolds for bone tissue engineering applications

H. Pereira^{a,b,c,*}, I.F. Cengiz^{a,b}, F.R. Maia^{a,b}, F. Bartolomeu^c, J.M. Oliveira^{a,b}, R.L. Reis^{a,b}, F. S. Silva^c

^a 3B's Research Group, I3Bs – Research Institute on Biomaterials, Biodegradables and Biomimetics, University of Minho, Headquarters of the European Institute of Excellence on Tissue Engineering and Regenerative Medicine, AvePark-Parque de Ciência e Tecnologia, Zona Industrial da Gandra, 4805-017, Barco, Guimarães, Portugal

^b ICVS/3B's – PT Government Associate Laboratory, Braga/Guimarães, Portugal AvePark, 4805-017, Barco, Guimarães, Portugal

^c Center for MicroElectroMechanical Systems (CMEMS-UMinho) – University of Minho, Campus de Azurém, Portugal

ARTICLE INFO

Keywords:

Ti₆Al₄V scaffolds
ZrO₂ scaffolds
PEEK scaffolds
SaOS-2 cells
Bone tissue engineering

ABSTRACT

Bone is a dynamic tissue with an amazing but yet limited capacity of self-healing. Bone is the second most transplanted tissue in the world and there is a huge need for bone grafts and substitutes which lead to a decrease in bone banks donors. In this study, we developed three-dimensional scaffolds based on Ti₆Al₄V, ZrO₂ and PEEK targeting bone tissue engineering applications. Experimental mechanical compressive tests and finite element analyses were carried out to study the mechanical performance of the scaffolds. Overall, the scaffolds presented different hydrophilicity properties and a reduced elastic modulus when compared with the corresponding solid materials which can in some extension minimize the phenomenon of stress shielding. The ability as a scaffold material for bone tissue regeneration applications was evaluated *in vitro* by seeding human osteosarcoma (SaOS-2) cells onto the scaffolds. Then, the successful culture of SaOS-2 cells on developed scaffolds was monitored by assessment of cell's viability, proliferation and alkaline phosphatase (ALP) activity up to 14 days of culturing. The *in vitro* results revealed that Ti₆Al₄V, ZrO₂ and PEEK scaffolds were cytocompatible allowing the successful culture of an osteoblastic cell line, suggesting their potential application in bone tissue engineering.

Statement of Significance.

The work presented is timely and relevant since it gathers both the mechanical and cellular study of non-degradable cellular structures with the potential to be used as bone scaffolds. This work allow to investigate three possible bone scaffolds solutions which exhibit a significantly reduced elastic modulus when compared with conventional solid materials. While it is generally accepted that the Ti₆Al₄V, ZrO₂ and PEEK are candidates for such applications a further study of their features and their comparison is extremely important for a better understanding of their potential.

1. Introduction

Bone is a complex, hierarchic and dynamic tissue with a remarkable capacity of self-healing, nevertheless, when a defect exceeds a critical size it loses the capacity of repairing and clinical intervention is needed (Rasheed et al., 2019). Current strategies used for the treatment of bone defects such as *Masquelet* technique or the use of autografts requires invasive bone collection with donor site morbidity as well as painful surgical procedures. In fact, bone is considered one of the most common tissue transplantation procedure after blood and kidney (Giwa et al.,

2017; Morelli et al., 2016). Bone tissue engineering (BTE) approaches are demanded to overcome the limitations of current solutions. A key component in BTE is the scaffold structure once its architecture works as a guide for cell interactions and the formation of the bone-extracellular matrix which provides structural support to the newly formed tissue.

In order to achieve a successful bone engineered scaffold, it is imperative to understand bone structure and biomechanics which vary with age, site and bone quality (Boskey and Robey, 2018). There are various mechanical properties that can describe bone tissue but the most important in the conception of bone scaffolds is the stiffness of the

* Corresponding author. ICVS/3B's – PT Government Associate Laboratory, Braga/Guimarães, Portugal AvePark, 4805-017, Barco, Guimarães, Portugal.
E-mail address: helena.frs.pereira@gmail.com (H. Pereira).

<https://doi.org/10.1016/j.jmbbm.2020.103997>

Received 14 January 2020; Received in revised form 8 July 2020; Accepted 16 July 2020

Available online 9 August 2020

1751-6161/© 2020 Elsevier Ltd. All rights reserved.

material which can be assessed through the elastic modulus (Wang et al., 2016). The elastic modulus of trabecular bone goes from 0.02 to 2 GPa and of compact bone can vary between 3 and 30 GPa (Yang et al., 2001). They should not collapse during the surgical procedure either patient's life. Nevertheless, it is necessary that the scaffold presents a proper elastic modulus to avoid bone resorption - stress shielding (Iqbal et al., 2019; Leong et al., 2008).

Several materials are used as base materials for scaffolds, metallic biomaterials due to their mechanical properties and corrosion resistance are mainly used for the fabrication of scaffolds for the replacement of hard tissue, such as artificial hip joints, bone plates, and dental implants (Niinomi, 2003; Gilbert, 2017). Titanium alloys, in particular, Ti₆Al₄V alloy is commonly used due to its excellent corrosion resistance and their modulus of elasticity of ~110 GPa. Ceramics are generally defined as inorganic, non-metallic materials. Ceramics such as alumina and zirconia ceramics are the most used in orthopedic devices. Zirconia combines high strength and fracture toughness with an attractive biocompatibility. Tetragonal zirconia, ZrO₂, especially 3% Yttria stabilized has been used as a conventional material for medical restorations due to its mechanical properties with an elastic modulus of 200 GPa (Denry and Kelly, 2008). Synthetic polymeric biomaterials are much more easily reproducible. Poly-ether-ether-ketone, PEEK, is a semi-crystalline polymer with high chemical resistance and it also presents high fracture toughness. But the major beneficial property for orthopedics application is its lower elastic modulus 3–4 GPa (Rae et al., 2007).

The scaffold's architecture is critical and pores play a key role once it allows cells penetration, growth, proliferation and differentiation. It has been shown previously by Kuboki et al. the importance of porous scaffolds for the formation of new tissue (Kuboki et al., 1998; Wu et al., 2014). Additionally, studies have shown better results in pore size greater than 300 µm for bone ingrowth (Bohner et al., 2011; Karageorgiou and Kaplan, 2005; Murphy et al., 2010; Jones et al., 2004). Although the pore size of a scaffold is crucial for the success of scaffold's performance, it becomes conflicting with other properties, once the increase of pore size affects directly the strength of the scaffold.

In this reasoning, the purpose of this study was to evaluate three different types of scaffolds, Ti₆Al₄V produced by Selective Laser Melting and commercial ZrO₂ and PEEK materials, in order to assess their potential for bone tissue engineering applications. CNC milling was used to create the desired architecture in the ZrO₂ and PEEK materials. The physicochemical properties of the developed scaffolds were investigated. The elastic modulus and compressive stress of the scaffolds were assessed by means of experimental compressive testing and finite element analyses were also performed for comparison purposes. The crystallographic phase of ZrO₂ was investigated by X-ray diffraction analyses, and the chemical composition of the scaffolds was assessed by means of using X-ray photoelectron spectroscopy technique. Surface characterization of the scaffolds was performed by carrying out Micro CT, SEM as well as roughness. In order to analyze the scaffolds wettability contact angle was performed.

The scaffolds architecture was also determined by micro-computed tomography analyses. Finally, the scaffolds biological performances were investigated *in vitro*. Human osteosarcoma (SaOS-2) cells were seeded and cultured onto the surface of the three types of scaffolds, and cells adhesion, viability, proliferation and ALP activity were evaluated.

2. Materials and methods

2.1. Scaffolds preparation

In this study open-cellular structures were produced with an open pore size of 400 µm, these structures were designed having throughout holes. The Ti₆Al₄V scaffolds were fabricated using a commercial Selective Laser Melting equipment from SLM Solutions (model 125HL). The production occurred under an Argon atmosphere, using a platform at a constant temperature of 200 °C and using the processing parameters

detailed described elsewhere (Bartolomeu et al., 2016). The average pore size obtained was of 375 µm.

ZrO₂ and PEEK porous specimens with 5 mm of height and with an average pore diameter of 400 µm were produced by CNC milling (Roland DWX-50). ZrO₂ used to produce the scaffolds was *Zirconia commercial Dental Direkt Bio ZW iso* and for PEEK was *PEEK commercial Dental Direkt Peek MED*. The cutting tool used to produce the porous scaffolds of ZrO₂ was made of hard metal with a 0.5 mm diameter spherical top. During the process the cutting tool penetrates 0.20 mm, rises and then penetrates a further 0.20 mm and so on until the hole is completed (feedrate), its rotation speed is 30000 rpm. The speed rate used was 5 mm s⁻¹. After machined the samples are cleaned and sintered using a stage at 1500° for 2 h with heating and cooling rates of 8 °C min⁻¹. To machined PEEK samples a cutting tool used was made of hard metal with a 0.4 mm diameter spherical top and a speed rate of 30000 rpm. The speed rate used was 8 mm s⁻¹ and the feedrate of the cutting tool was 0.10 mm. After processing all samples were ultrasonically cleaned in isopropanol for 10 min in order to remove any loose debris or surface contamination. The pore size was of 390 µm for ZrO₂ and for PEEK.

2.2. Physicochemical characterization

2.2.1. X-ray diffraction

The qualitative analyses of crystalline phases presented on the samples were obtained by X-ray diffraction (XRD) using a conventional Bragg-Brentano diffractometer (*Bruker D8 Advance DaVinci, Germany*) equipped with CuK α radiation, produced at 40 kV and 40 mA. Data sets were collected in the 2 θ range of 10–60° with a step size of 0.02° and 1s for each step.

2.2.2. X-ray photoelectron spectroscopy

Surface chemistry of each scaffold material was analyzed by X-ray photoelectron spectroscopy (XPS) using Axis Supra for the elemental composition of the scaffolds. The XPS analysis of a surface provides qualitative and quantitative information on all the elements present (except H and He) from the binding energies of the main lines and the peak area, respectively. Three regions were located in each scaffold and the analyzer was used at the constant ΔE mode with 20 eV pass energy.

2.2.3. X-ray micro-computed tomography

The quantitative and qualitative evaluation of the scaffolds' structure were performed using a high-resolution X-ray micro-computed tomography system Skyscan 1272 (*Skyscan, Kontich, Belgium*). The scanning of the scaffolds was conducted using a pixel size of 5 µm and an X-ray source fixed at 50 keV and 200 µA. The two-dimensional (2D) images in each data set were binarized automatically using the manufacturer's software (*CT Analyzer v1.17, SkyScan, Kontich, Belgium*). Formerly, the images were used for morphometric analysis by quantification of mean porosity, mean pore size, mean wall thickness. The porosity, pore size and wall thickness were also determined on the 2D images. Three samples were used for the qualitative and quantitative microstructure evaluation.

2.2.4. Surface roughness

The polishing was performed using a MECAPOL P251 and different types of sandpapers with different meshes. With this procedure, the purpose was to polish the surface of the samples in order to obtain smoother surfaces. The series of sandpapers used for polishing all the samples were: Ti₆Al₄V specimens were polished with P4000 grit size, ZrO₂ with grit from P180 to P4000 size and PEEK samples were polished with P600 to P4000 grit size and then further polish was complete using a diamond suspension with a particle size of 3 µm (*DiaPro Dur*). The roughness of both polished and processed surfaces was measure by means of profilometry (*Mitutoyo SJ 210*). Throughout the test, the rugosimeter's needle dislocated horizontally with a 6 µs speed along the length of the sample with measurements being acquired in every 2.5 µm

of dislocation. The presence of micro peaks and valleys, during the roughness measurement, created vertical movements in the touch probe that was, then, converted by the existing transducer into electrical signs and these were amplified vertically and horizontally being converted later into dimensional values.

2.2.5. Contact angle and surface energy analyses

Wettability can be defined as the propensity of liquid to spread on a solid surface and normally consist on the measurement of contact angles as the primary data, which indicates the degree of wetting when a solid and liquid interact. Contact angles were obtained using the sessile drop method with an instrument (*GONIOMETER OCA15+*), this fully automated apparatus, with integrated pump, delivers accurate droplets and the built-in camera captures an image to measure the static contact angle. All specimens were ultrasonically cleaned with alcohol before the measurement to minimize physical and chemical contamination of the surfaces. Distilled water was used for contact angle measurements. The calculations were performed at room temperature and the drop was put directly on the side surface of the holes. Diiodomethane (*Sigma-Aldrich Química, S.L., Portugal*) and distilled water were used for surface free energy calculations. Three drops were analyzed for each scaffold material. The final contact angle used for comparison of different samples was the average of the left and right angles of each drop.

2.2.6. Scanning electron microscopy

To assess the microstructure of the different materials the scaffolds and the ability to cells adhere and spread along the porous scaffolds surface scanning electronic microscope was used (*JEOL JSM-6010LV*). For that, the scaffolds were collected after 14 days of culture and fixed with 10% formalin for 20 min. Then they were washed with ultra-pure water three times. The samples were then dehydrated in increased concentrations of ethanol from 30% to 100% and air-dried overnight. Before observed in SEM, the specimens were coated with gold.

2.2.7. Mechanical analyses

In order to assess the mechanical performance of the $\text{Ti}_6\text{Al}_4\text{V}$, ZrO_2 and PEEK scaffolds produced in this study, experimental compressive tests were performed using an universal testing machine (Instron 874, USA). The tests were made at room temperature and the load direction was parallel to the direction of the holes of the scaffolds. The load gauge of the universal testing machine was used for load signal acquisition and three samples were used for each scaffold typology. The tests were performed with a 0.005 mm/s crosshead speed and the strain signal was obtained using a dynamic extensometer from Instron (model 2620–601). The elastic modulus was estimated using the elastic regime slope of the stress-strain plots.

Finite element analyses were carried out to simulate compression stress-strain tests and to compare the obtained results with the experimental data. A structural mechanical module was set for the mechanical simulation and the structures were modelled as a linear elastic materials using the micro-CT and SEM morphological data. The models were defined with an elastic modulus, Poisson's ratio and density of 110 GPa, 0.34 and 4500 kg/m³ for the $\text{Ti}_6\text{Al}_4\text{V}$, 200 GPa; 0.30 and 6000 kg/m³ for the ZrO_2 ; 3.76 GPa, 0.38 and 1300 kg/m³ for PEEK (Bartolomeu et al., 2019; Kubota et al., 2014; Garcia-Gonzalez et al., 2015). Finite element meshes were generated for each model using tetrahedral elements following the same strategy as reported in literature (Bartolomeu et al., 2019), assuring the convergence of the numerical simulation following a parametric study.

2.3. Scaffolds in vitro characterization

2.3.1. Cell culturing

A human osteosarcoma - derived cell line (SaOS-2) was used to perform the *in vitro* studies. SaOS-2 cells were expanded until 90% confluence using basic culture medium Dulbecco's modified Eagle's –

DMEM - with 10% fetal bovine serum (*Life Technologies Europe BV, Netherland*) and 1% antibiotic/antimycotic (*Life Technologies, Scotland*) solution.

The scaffolds were transferred to non-adherent 48-well plates where the air inside the scaffolds was removed by flushing medium through the pores. Afterwards, the SaOS-2 cells were detached with TripleTEM Express with Fenol Red. A cell suspension was prepared (33.19×10^6 cells. mL⁻¹) and seeded onto the scaffolds in a drop-wise manner, at a cellular density of 200 million cells per scaffold. After 3 h, 500 μL of culture medium was added to the well plates. A control was prepared by seeding 10×10^3 cells per well in adherent 12-well plates and maintained under the same conditions and for the same period. The medium was changed twice a week during the time of the experiment.

2.3.2. Cell viability

Samples were collected on days 1, 3, 7 and 14 after seeding for the assessment of cell viability by Alamar blue test (*Bio-Rad, UK*). For that, a solution with 10% of Alamar blue (*Bio-Rad, UK*) was prepared, added to each well and incubated for 3 h at 37 °C. Afterwards, 100 μL were transferred to a well of a 96-well black plate and the fluorescence was read at an excitation of 530/25 nm and an emission of 590/35 nm using a microplate reader (*Gen 5 2.01, Synergy HT*).

2.3.3. Cells proliferation

Cell proliferation was assessed by DNA quantification. For that, scaffolds used for Alamar blue assay were washed with PBS and transferred into 1.5 mL microtubes containing 1 mL ultra-pure water. The control with the 2D seeded cells was washed with PBS and then 1 mL of ultra-pure water was added. Then, both scaffolds and 2D control were incubated for 1 h at 37 °C. Concerning 2D control, the volume of each well was transferred into a 1.5 mL microtubes. Then, all samples were stored in a –80 °C freezer, promoting a thermal shock and thus potentiating the cell lyses. Additionally, before DNA quantification, cell lysates were defrosted at room temperature and then sonicated in an ultrasonic bath for 15 min. Finally, DNA concentration was quantified by using the kit Quant-IT PicoGreen dsDNA Assay kit 2000 assays (*Life Technologies, Scotland*), accordingly with manufacturer's instructions. Briefly, 28.7 μL of sample or standard, 71.3 μL of PicoGreen solution and 100 μL of Tris–HCl–EDTA buffer were mixed in each well of an opaque 96-well plate and were incubated in the dark for 10 min. Triplicates were made for samples and standards. After that, fluorescence was measured using an excitation wavelength of 485 nm and an emission wavelength of 530 nm. A DNA standard curve was prepared with concentrations varying between 0 and 2 $\mu\text{g mL}^{-1}$ and sample DNA values were read off from the standard graph.

2.3.4. Alkaline phosphatase activity

For Alkaline phosphatase (ALP) activity assessment, molecular absorbance spectrophotometry measurement and Fast Violet B staining was performed. Concerning the first, for the quantification of ALP activity cell lysates produced for DNA quantification were used. Briefly, 20 μL of each sample and 60 μL of substrate solution (0.2% w/v p-nitrophenyl phosphate (pnPP) in 1 M Diethanolamine) were added to each well of a transparent 96-well plate and incubated in the dark for 45 min at 37 °C. Then, 80 μL of a solution to stop the reaction composed of 0.2 M NaOH and 0.2 mM EDTA was added to each well. Absorbance was read at 405 nm using a microplate reader (*Gen 5 2.01, Synergy HT*). A p-nitrophenol standard curve was prepared with concentrations varying between 0 and 0.2 nmol mL⁻¹ and sample values were read off from the standard graph.

In the case of ALP staining, after 14 days of culture, cells were fixed with 10% formalin for 20 min and stained with Fast violet B (*Sigma-Aldrich Química, S.L., Portugal*) with Naphthol (*Sigma-Aldrich Química, S.L., Portugal*). In this sense, as a result of phosphatase activity, Naphthol is liberated and immediately coupled with a diazonium salt, forming an insoluble, visible pigment at sites of phosphatase activity. For that, a

mixture of both reagents was prepared and added to each sample. After 1 h of incubation at 37 °C, the solution was removed, washed with PBS and air-dried. The images of the staining were taken in a Stereo Microscope (Stemi, 2000-C Zeiss).

2.4. Statistical analysis

Statistical analyses were performed using GraphPad Prism 5.0 software version 5.0a. The non-parametric Mann–Whitney test was used to compare two groups, whereas the comparison between more than two groups was performed using the Kruskal–Wallis test followed by Dunn's comparison test. A value of $p < 0.05$ was considered statistically significant. Data are presented as mean \pm standard deviation. Data in each figure are from three independent experiments each one with $n = 3$.

3. Results

3.1. Physicochemical characterization

3.1.1. X-ray diffraction

The X-ray Diffraction (XRD) was used to identify the crystalline phase of ZrO₂ scaffolds. As depicted in Fig. 1, the ZrO₂ scaffolds showed the typical intensity peaks corresponding to the tetragonal ZrO₂ phase (marked with *), with good consistency with their respective ICDD standard card 00-060-0502.

3.1.2. X-ray photoelectron spectroscopy

In order to obtain information about the surface-near chemistry, all samples were analyzed by X-ray photoelectron spectroscopy (XPS) as depicted in Figs. 2–4. Fig. 2A shows the survey scan of Ti₆Al₄V scaffolds, showing the typical peaks of Oxygen (O) 1s, Titanium (Ti) 2p and Carbon (C) 1s, as expected. Additionally, a high-resolution XPS spectrum of Ti₆Al₄V scaffolds was obtained (Fig. 2B), where it is possible to observe a peak with the binding energy of 458.7 eV, corresponding to metallic titanium (Ti 2p).

In the case of ZrO₂ scaffolds, XPS analysis is shown in Fig. 3. The survey scan XPS spectrum of ZrO₂ scaffolds (Fig. 3A) showed a range of binding energies between 39.66 eV and 1205.66 eV with 4 different peaks that correspond to O 1s, Zirconium (Zr) 3p_{3/2}, Zr 3p_{1/2} and Zr 3d. Moreover, in the high-resolution XPS spectra of ZrO₂ scaffolds (Fig. 3B) is possible to see the peak of Zr 3d that presented an energy binding of 182.0 eV. Furthermore, in the high-resolution spectra was also possible to identify Yttria (Y) 3d with an energy binding of 157.0 eV (Fig. 3C), which was not visible in the survey scan due to its low quantity (3%).

The XPS spectra of PEEK is displayed in Fig. 4. As observed in Fig. 4A, the peaks of O 1s and C 1s were detected in the survey scan of PEEK, as expected for polymers. These peaks had an energy binding of 533.6 eV,

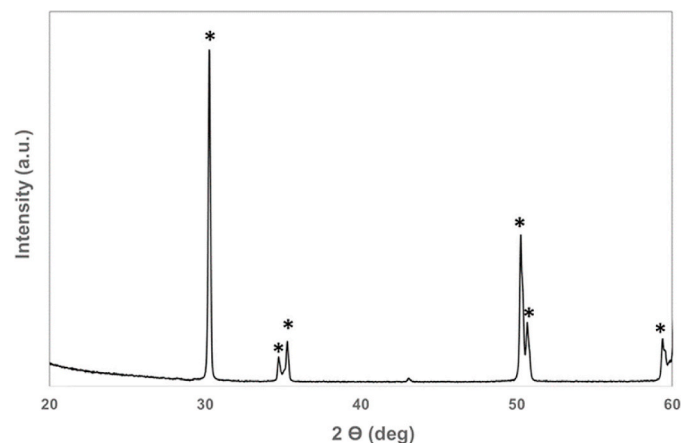


Fig. 1. XRD plot of tetragonal phase of ZrO₂.

in the case of O 1s, and 285.0 eV, in the case of C 1s, as depicted in the high-resolution XPS scan presented in Fig. 4B and C, respectively.

3.1.3. X-ray micro-computed tomography

The qualitative and quantitative analysis of porosity, mean pore size and mean pore thickness of the scaffolds were assessed by micro-CT (Table 2). Micro-CT histomorphometric analyses revealed no substantial differences in the mean porosity between the samples. As expected, significant differences were observed when comparing PEEK with Ti₆Al₄V samples in terms of mean wall thickness and mean pore size. In this sense, PEEK samples presented higher values of mean wall thickness and mean pore size.

3.1.4. Surface roughness

Another parameter analyzed was the surface roughness (Ra) as presented in Table 3. The machined scaffolds analyzed by profilometry showed a surface roughness of Ra = 0.966 μ m for Ti₆Al₄V, Ra = 2.03 μ m for ZrO₂ and Ra = 1.051 μ m for PEEK. After the polishing of the scaffolds, the average values of surface roughness significantly decreased ($p = 0.0015$), as expected. In this sense, the values obtained were Ra = 0.144 μ m for Ti₆Al₄V; Ra = 0.013 μ m for ZrO₂; and Ra = 0.192 μ m for PEEK.

3.1.5. Contact angle and surface energy

Contact angles were also assessed as shown in Table 4. The values were obtained by the sessile drop method on the different surfaces before (i.e. machined) and after (i.e. polished) the scaffolds had been processed. In both conditions, machined and polished, ZrO₂ samples demonstrated similar contact angles values, which were lower than 90°, indicating that these scaffolds presented a hydrophilic surface. Whereas, machined and polished Ti₆Al₄V and PEEK samples showed similar contact angles higher than 90°, which correspond to hydrophobic surfaces.

Additionally, the surface energy of rough and polish surfaces was studied and the values obtained are presented in Table 5. As shown, the values of surface energy increased for Ti₆Al₄V and PEEK samples after the polishing, while in the case of ZrO₂ samples, the surface energy is decreased.

3.1.6. Mechanical analyses

The stiffness of materials for bone tissue engineering approaches is a crucial parameters once it defines the behavior of the material under mechanical loading. In this sense, the three scaffolds typologies (Ti₆Al₄V, ZrO₂ and PEEK) investigated in the present study were mechanically tested under compression loading as mentioned before. The elastic modulus results of the experimental tests and the finite element analyses can be seen in Fig. 5.

When analyzing Fig. 5, several aspect can be pointed. As expected, significantly lower elastic modulus were obtained for the Ti₆Al₄V, ZrO₂ and PEEK scaffolds when compared with the based solid materials. When regarding the experimental results, the Ti₆Al₄V scaffolds exhibit elastic modulus of 76.85 ± 1.43 GPa, while the ZrO₂ and PEEK scaffolds show an elastic modulus of 141.70 ± 1.04 GPa and 2.78 ± 0.06 GPa, respectively. These results are relevant when thinking about the application of these scaffolds in bone tissue engineering solutions for reducing the stress shielding phenomena (Nagels et al., 2003). The obtained elastic modulus values are aligned with literature taking into account a porosity of $\pm 38\%$ as reported in Table 2. Moreover, it can be observed in Fig. 5 that the identical elastic modulus values were obtained when comparing the experimental testing with the finite element analyses, which validates both of the studies approaches, similarly to those observed in reported studies of these group of authors (Bartolomeu et al., 2019, 2020).

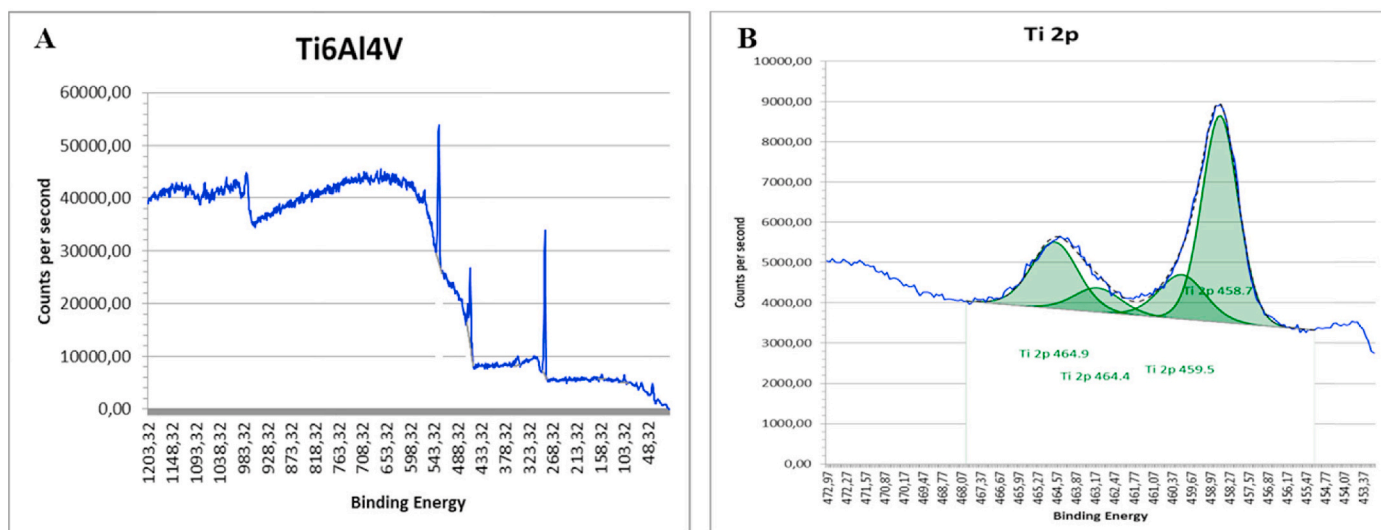


Fig. 2. XPS plot of Ti₆Al₄V. A) Survey scan XPS spectra; and B) high-resolution XPS spectra of Ti₆Al₄V showing the peak of Ti 2p.

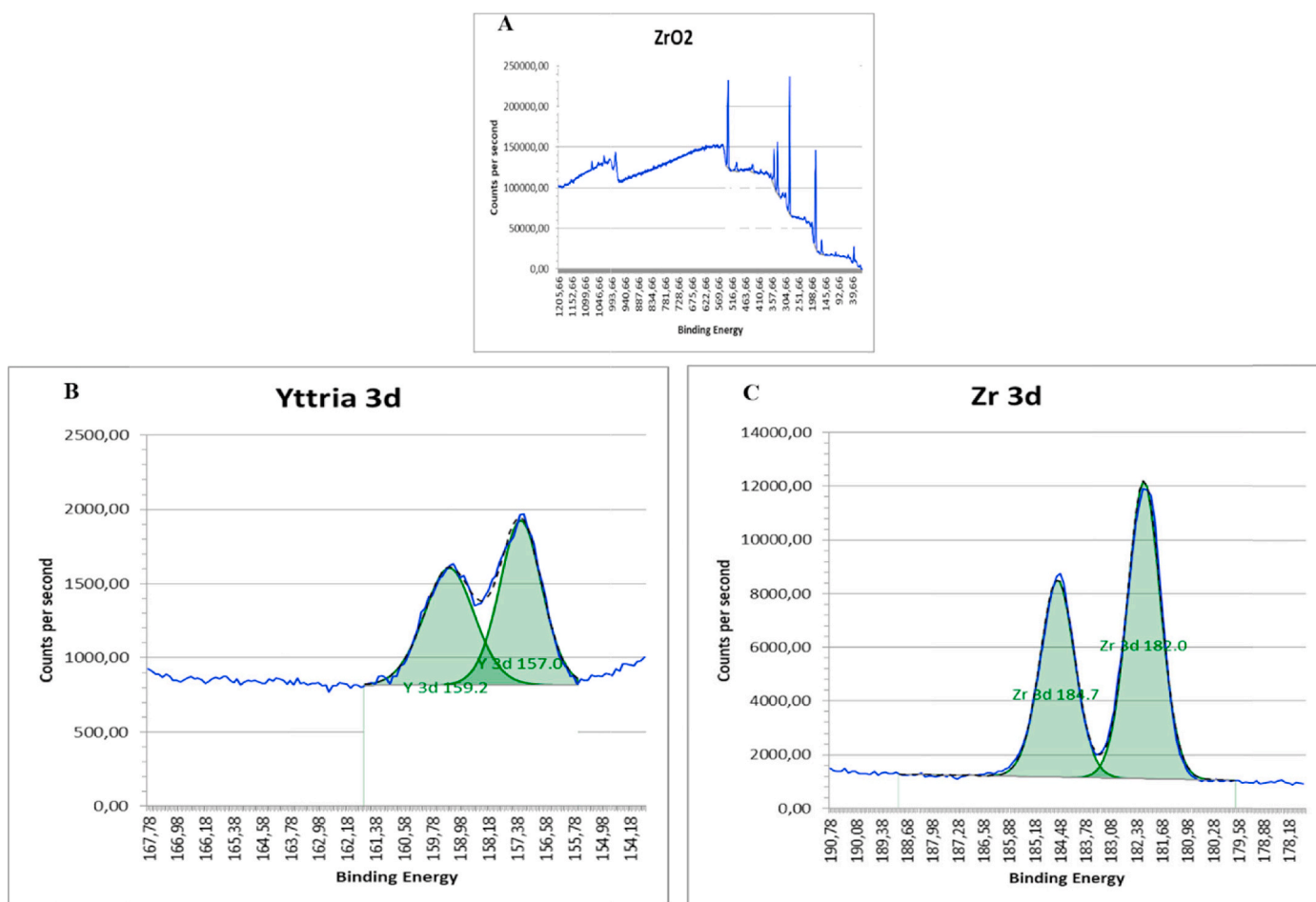


Fig. 3. XPS plot of ZrO₂. A) Survey scan XPS spectra showing to O 1s, Zr 3p_{3/2}, Zr 3p_{1/2} and Zr 3d peaks; B) high-resolution XPS spectra of Y 3d; and C) high-resolution XPS spectra of Zr 3d.

3.2. Biological characterization

3.2.1. Cells adhesion and spreading

Cell adhesion and spreading were visualized by Scanning electron microscopy (SEM) as depicted in Fig. 6. In Fig. 6 a-c, it is possible to

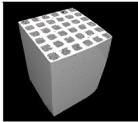
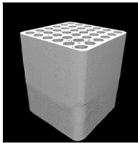
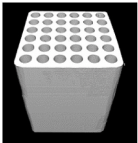
observe the unseeded scaffolds, which presented an average height of 5 mm. After the seeding of SaOS-2, it was possible to clearly observe that cells adhered to the surface (Fig. 6 g, h and i) when compared with unseeded scaffolds. Looking more closely, it was visible that both, Ti₆Al₄V and ZrO₂, presented more cells adhered and spread throughout



Fig. 4. XPS plot of PEEK. A) Survey scan XPS spectra showing O 1s and C 1s peaks; B) high-resolution XPS spectra of O 1s; and C) high-resolution XPS spectra of C 1s.

Table 2

3D reconstructions of Ti₆Al₄V, ZrO₂ and PEEK samples, mean porosity and trabeculae thickness, calculated from the micro-CT data, presented as mean ± standard deviation.

Material	Scaffold image reconstruction	Mean porosity (%)	Mean wall thickness [μm]
Ti ₆ Al ₄ V		38.0 ± 1.78	138.1 ± 4.62
ZrO ₂		39.4 ± 0.77	224.3 ± 7.07
PEEK		37.3 ± 0.74	250.1 ± 6.83

their surface when compared with PEEK scaffold surface (Fig. 6 d, e and f). As observed Ti₆Al₄V scaffolds present a quite high surface which should promote cell adhesion of SaOS-2.

Table 3

Mean ± standard deviation values of Ra for machined and polished samples.

Type of scaffolds	Processed (μm)	Polished (μm)
Ti ₆ Al ₄ V	0.966 ± 0.13	0.144 ± 0.02
ZrO ₂	2.030 ± 0.35	0.039 ± 0.02
PEEK	1.501 ± 0.39	0.192 ± 0.07

Table 4

Contact angle measurement values of machined and polished samples.

Machined Sample	Contact angle (θ)	Sample Polished	Contact angle (θ)
Ti ₆ Al ₄ V	102.70 ± 10.72	Ti ₆ Al ₄ V	90.2 ± 12.29
ZrO ₂	78.75 ± 5.57	ZrO ₂	83.85 ± 8.24
PEEK	99.05 ± 9.65	PEEK	96.15 ± 3.24

Table 5

Surface energy measurement values of machined and polished samples.

Machined Sample	Surface Energy (mN. m ⁻¹)	Polished Sample	Surface Energy (mN. m ⁻¹)
Ti ₆ Al ₄ V	18.20	Ti ₆ Al ₄ V	25.16
ZrO ₂	31.68	ZrO ₂	29.8
PEEK	30.55	PEEK	34.36

3.2.2. Cells viability

The Alamar blue results elucidate about the cells' metabolic activity, which consequently can be transduced in cell viability. In this sense,

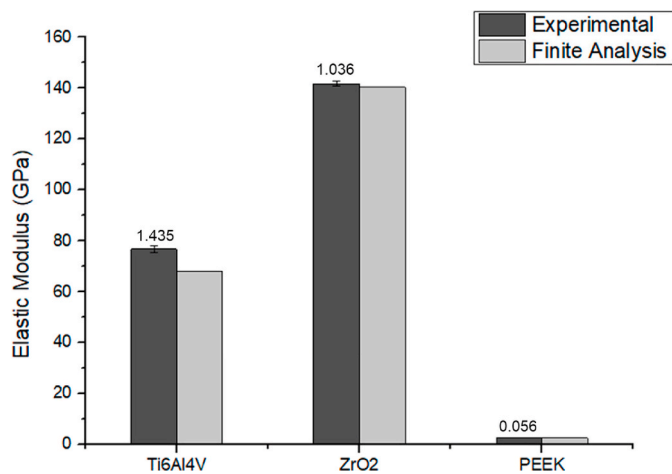


Fig. 5. Elastic modulus obtained from experimental tests and finite element analysis.

cells are able to metabolize resazurin, the active ingredient of Alamar blue reagent, and reduce it into resorufin, a compound that is red in color and highly fluorescent. When viable cells convert resazurin to resorufin, the overall fluorescence of the media surrounding cells, increases. The results obtained along the 14 days of culture of SaOS-2 cells in 2D standard cultures (2D-Control) and on the scaffolds were normalized by DNA concentration and are presented in Fig. 7. As shown, after 1 day, cells cultured on Ti₆Al₄V scaffolds and 2D-Control were more metabolic active when compared with ZrO₂ and PEEK scaffolds. Nevertheless, the metabolic activity of these same cells decreased after 14 days of culture, while cells cultured on ZrO₂ and PEEK scaffolds presented similar values to day 1. Concerning ZrO₂ and PEEK scaffolds, although no differences between them were detected on day 1, cells cultured on ZrO₂ scaffolds showed to be more active than cells cultured on PEEK scaffolds on day 14. Noteworthy, the values presented by cells cultured in 2D-Control at day 14 were significantly lower than cells cultured on scaffolds. It is important also to point out that, in 2D-Control, cells were more metabolic active along the first 7 days of culture, decreasing on day 14.

3.2.3. Cells proliferation

Cells proliferation was assessed by DNA quantification along the 14 days of culture of SaOS-2 cells on 2D standard cultures and scaffolds, as depicted in Fig. 8. At day 1 there is a clear difference between 2D control and scaffolds, which can be explained by the different cell concentration used for both conditions. Along the 14 days of culturing, although cells under all conditions proliferated, higher DNA content was observed in 2D control as compared with scaffolds. Interestingly, cells cultured on ZrO₂ scaffolds showed higher proliferation rates than cells cultured on PEEK scaffolds and slightly higher than Ti₆Al₄V scaffolds at day 1. But at day 14, cells showed an opposite proliferation rate, being significantly lower than Ti₆Al₄V and PEEK cell scaffolds.

3.2.4. Alkaline phosphatase activity

Alkaline phosphatase (ALP) activity is an early osteoblastic phenotypic marker and an indicator of the osteoblastic behavior of SaOS-2 cells (Postiglione et al., 2003). For so, ALP activity (normalized by DNA content) was evaluated by molecular absorbance spectrophotometry measurement and by staining with Fast Violet B (Figs. 9 and 10), respectively. Considering ALP measurements on day 3, values were similar for all conditions. However, ZrO₂ scaffolds showed higher values when compared with 2D control. Considering the values of day 7, cells on 2D control had higher activity than day 3, which decreased until day 14, showing the typical peak of expression. Moreover, the values of ALP activity of 2D control were higher than scaffolds, while amongst the

scaffolds, cell-seeded Ti₆Al₄V and ZrO₂ showed higher values than cell-seeded PEEK scaffolds. In the case of ALP activity at day 14, all conditions showed lower values than day 3 and day 7, however, ALP qualitative activity was still detected by Fast Violet B staining as depicted in Fig. 10. Interestingly, 2D control showed the lowest values at this time point. Once more, Ti₆Al₄V scaffolds showed higher values than PEEK and ZrO₂ scaffolds, which was corroborated by the ALP staining (Fig. 10).

4. Discussion

Tissue engineering approaches have been essential for the development of some commercially available products for the use in bone defects treatments (Infuse; Vitoss). But none of those products is able to induce bone regeneration. In fact, for bone applications, it is crucial to have proper mechanical properties and have the capacity to host cells. A common problem with currently available solutions is their mismatch with bone in terms of elastic modulus. It has been reported that when elastic modulus, between an implant and bone, presents a mismatch, stress transfer happens. This phenomenon calls stress shielding and leads to bone reabsorption (Bartolomeu et al., 2016; Navarro et al., 2008). One approach to solve such problem is to reduce the elastic modulus of materials by introducing pores. Additionally, the introduction of pores presents another advantage for the scaffolds as it facilitates cell penetration, tissue ingrowth and vascularization.

In the presented study, three dimensional (3D)-scaffolds, with different material compositions, Ti₆Al₄V, ZrO₂ and PEEK, with a pore size of 400 μm chosen according to studies previously published were prepared (Zhang et al., 2016; Im et al., 2012). They were evaluated regarding their surface's characteristics, mechanical properties, and influence in the cell. XRD was performed to assess the crystallographic phase of ZrO₂ scaffolds after processing. In fact, ZrO₂ can present three crystallographic phases: monoclinic (m), tetragonal (t), and cubic (c), being the tetragonal the more stable phase for ZrO₂ (Denry and Kelly, 2008). Each crystallographic phase can develop during heating or cooling processes. As we can observe in 4-1 the ZrO₂ XRD plot presents a typical tetragonal phase plot, indicating that the ZrO₂ materials used during this study were stable and is in agreement with published data related to the tetragonal phase of ZrO₂ (Tsunekawa et al., 2005; Watanabe and Yoshinari, 2016). For the chemical composition, XPS analyzed were performed. The peaks of Ti, Zr, C and O were identified, as expected and reported elsewhere (Tsunekawa et al., 2005; Watanabe and Yoshinari, 2016; Shard and Badyal, 1992; Lu et al., 2015).

Furthermore, the micro-CT analysis was used to assess porosity, mean pore size and mean pore thickness of the scaffolds. As expected the porosity was similar in all scaffolds. The observed differences between the value obtained by the analysis of micro CT and the theoretical value are due to the constraint of the scaffold when sintering it after machining. The scaffolds suffer a shrinkage of 3%.

There are several topographical parameters that influence cells' behavior. For example, it was previously shown that contact angle and surface energy can influence the cell adhesion (Hallab et al., 2001). Moreover, the measurement of contact angles is extremely useful as they characterize the average of wettability of material's surface (Mohammed and Babadagli, 2015). Since all the scaffolds were polished, the influence of roughness on the wetting properties was evaluated by contact angle measurement analysis of rough and polished Ti₆Al₄V, ZrO₂ and PEEK samples. As it was observed on Table 3, rough ZrO₂ showed an angle lower than 90°, indicating that ZrO₂ exhibited a hydrophilic surface, whereas Ti₆Al₄V and PEEK, with an angle higher than 90°, exhibited a hydrophobic surface. Surface energy is also an important parameter in surface topography that influences biological response, once it is related with the wettability of the surface and thus its hydrophilicity. In fact, it is known that hydrophilic surfaces allow protein absorption to the implant surface and subsequent interaction with cells. In contrast, hydrophobic surfaces that are subjected to air bubbles

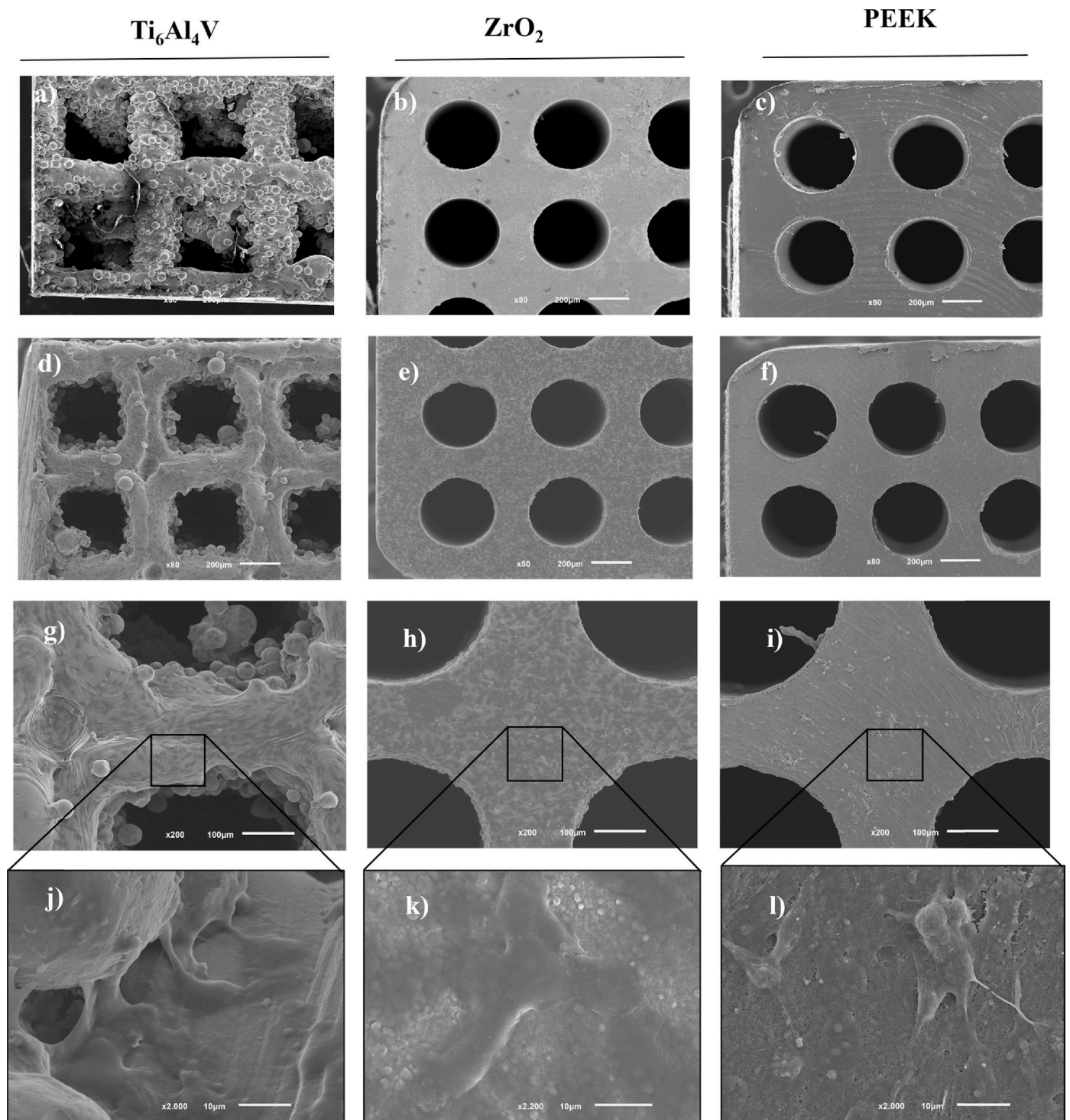


Fig. 6. SEM analysis. SEM image of a) unseeded $\text{Ti}_6\text{Al}_4\text{V}$ scaffold; b) unseeded ZrO_2 scaffold; c) unseeded PEEK scaffold; d) and g) seeded $\text{Ti}_6\text{Al}_4\text{V}$ scaffold; e) and h) seeded ZrO_2 scaffold f) and i) seeded PEEK scaffold; j) cell detail on seeded $\text{Ti}_6\text{Al}_4\text{V}$; k) cell detail on seeded ZrO_2 and l) cell detail on seeded PEEK.

entrapment hinder forbidding protein absorption and thus cell adhesion. In this context, many studies have concluded that a moderate hydrophilicity improves the biological response (Gittens et al., 2014).

Finally, the last property analyzed were the mechanical properties assessed by the elastic modulus analysis. In the literature is possible to find that the typical values of elastic modulus for bulk $\text{Ti}_6\text{Al}_4\text{V}$, ZrO_2 and PEEK materials are: 110 GPa; 200 GPa and 3.76 GPa, respectively (Osman and Swain, 2015; Najeeb et al., 2016; Jung et al., 2014). During the compression test, all scaffold presented a typical stress-strain curve.

As expected taking into consideration the level of porosity, the elastic modulus obtained when tested the scaffolds was about 30% lower than in bulk structure as shown in Fig. 5 and were in agreement with previous data published (Weißmann et al., 2016). In fact, these results validate the approach developed in this study and it should be highlighted that by tailoring the pore sizes it can be produced scaffolds with an elastic modulus in the range of cortical bone, between 3 GPa and 30 GPa.

After physicochemical properties analysis, cells' behavior was assessed. For that, osteosarcoma - derived cell line (SaOS-2) was used

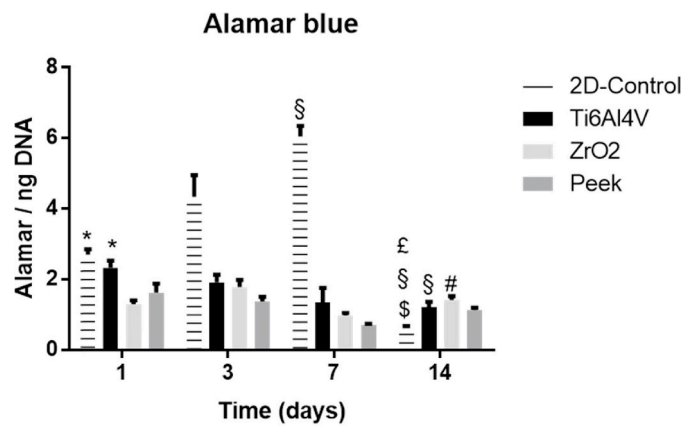


Fig. 7. SaOS-2 cells' metabolic activity normalized by DNA concentration, along 14 days of culture. Symbols denote statistically significant differences ($p < 0.05$) in comparison to: (*) ZrO₂ and PEEK scaffolds, (\$) scaffolds; (#) PEEK scaffolds; (£) day 7; and (§) day 1. Data is presented as mean \pm stdev ($n = 3$).

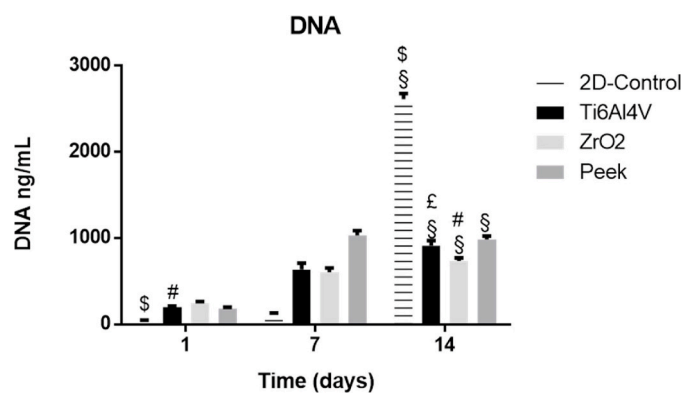


Fig. 8. SaOS-2 cells' proliferation rates by DNA concentration, along 14 days of culture. Symbols denote statistically significant differences ($p < 0.05$) in comparison to: (\$) scaffolds; (#) PEEK scaffolds; (§) day 1; and (£) ZrO₂ scaffolds. Data is presented as mean \pm stdev ($n = 3$).

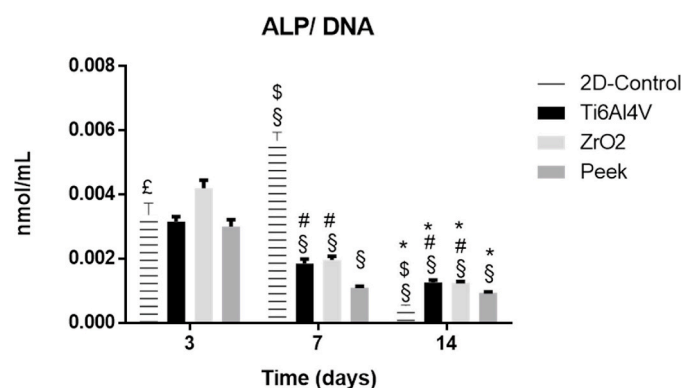


Fig. 9. SaOS-2 cells' ALP activity along 14 days of culture. Symbols denote statistically significant differences ($p < 0.05$) in comparison to: (£) ZrO₂ scaffolds; (\$) scaffolds; (§) day 3 (#) PEEK scaffolds; and (*) day 7. Data is presented as mean \pm stdev ($n = 3$).

since it was more physiologically relevant when considering the ultimate application. SaOS-2 cells, a good and well-characterized osteosarcoma human cell line, have been widely used as a model system for osteoblastic cells mostly due to their exhibition of the entire differentiation sequence of osteoblastic cells (Postiglione et al., 2003; Hausser and

Brenner, 2005).

By observing SEM images in Fig. 6 it was possible to observe that cells were able to adhere and spread at some extent in each material. Nevertheless, it was noticed a higher cell adhesion and spreading in Ti₆Al₄V and ZrO₂ scaffolds when compared to PEEK scaffolds. This could be explained by the higher roughness presented by Ti₆Al₄V and ZrO₂ scaffolds, which was described to improve not only cell adhesion but also cell spreading (Huang et al., 2004; Yang et al., 2016).

In the case of cell viability evaluation, metabolic activity was assessed. As shown in Fig. 7, the metabolic activity of SaOS-2 cultured on standard 2D cultures (2D control) followed a normal profile. In this sense, cells' metabolic activity increased until day 7 and decreased until day 14. This trend may be related to the typical engagement of SaOS-2 cells along the osteoblastic lineage, resulting in a lower activity while differentiating. Considering the DNA quantification, it is possible to state that cells proliferated along the entire time of culture in all conditions.

Considering the application of these materials for bone tissue approaches, the monitor of SaOS-2 cells' osteogenic behavior upon culture on developed scaffolds was also a motif of study. In fact, the information about osteogenic differentiation markers, as alkaline phosphatase, are important to evaluate the influence of the different materials on the successful culture of osteoblastic cells, which can later provide important insights concerning the bone formation and implant osseointegration. Several studies suggest that SaOS-2 cells can present a decrease in cell proliferation and an increase in alkaline phosphatase activity depending on scaffolds' surface properties (Postiglione et al., 2003). Indeed, the 2D - control, as shown in Fig. 9, showed a typical development in terms of ALP activity, i.e. ALP activity peaked at day 7 and decreased, but cells were proliferating the entire time of culture. For so, one can conclude that in 2D, SaOS-2 cells presented a typical ALP activity as expected. In the case of Ti₆Al₄V, ZrO₂ and PEEK scaffolds, although cells expressed ALP the entire culture indicating a successful culture of SaOS-2 cells, as observed by ALP activity quantification and detection by staining, it decreased along the 14 days. One explanation for the low levels of ALP activity observed is the deficient cell-cell contact as reported in previous studies (Cao et al., 2015; Tang et al., 2010) and supported by the continuous increase in the proliferation rate throughout the experiment time. Another explanation is that this study was not realized in osteogenic differentiation conditions, i.e. in the presence of ascorbic acid, dexamethasone and β -glycerophosphate.

5. Conclusion

In this study, novel Ti₆Al₄V, PEEK and ZrO₂ scaffolds were prepared by SLM and CNC machining. The scaffolds exhibit a suitable porosity for bone applications and a significant decrease on the elastic modulus of the scaffolds was observed when compared with the respective solid materials, which can be considered a relevant result for bone applications. Their *in vitro* cytocompatibility and osteogenic ability were screened using SaOS-2 cells showing that scaffolds were non-cytotoxic and were able to host cells for the time of culture. Although complementary *in vivo* studies are necessary to evaluate the long-term biological performance and stability of the scaffolds in subcutaneous and orthotopic models, the obtained results indicated that the developed scaffolds are promising structures for bone tissue engineering applications.

CRedit authorship contribution statement

Conceptualization: J.M. Oliveira, F.S. Silva made the design of this study. **Investigation:** H. Pereira and I.F. Cengiz performed the surface characterization; H. Pereira and F. Maia performed the cytocompatibility assessment; H. Pereira and F. Bartolomeu performed the mechanical test and finite element analyses. **Supervision:** J.M. Oliveira, F. S. Silva. **Writing - original draft:** H. Pereira, I.F. Cengiz, F. Maia, J.M.

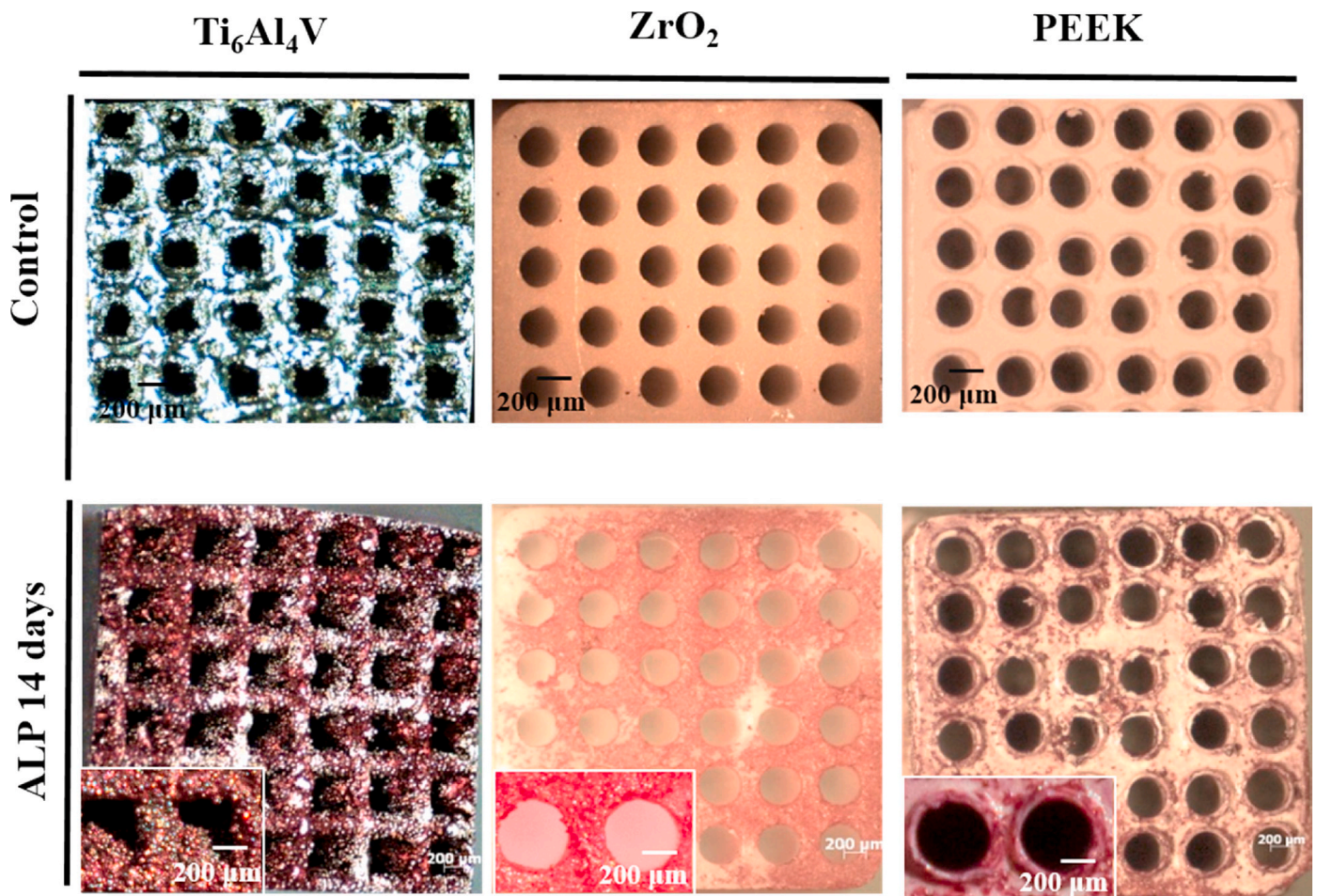


Fig. 10. ALP stained SaOS-2 cells on scaffolds and respective controls (scaffolds without cells) after 14 days of culturing. Insets show ALP stained cells on scaffolds at higher magnification.

Oliveira, F.S. Silva wrote the paper. **Writing - review & editing:** H. Pereira, I.F. Cengiz, F. Maia, J.M. Oliveira, F.S. Silva did the review and editing. **Resources:** R.L Reis, F.S. Silva, J.M. Oliveira (projects and individual grants).

Declaration of competing interest

The authors declare that they have no known competing financial interests or personal relationships that could have appeared to influence the work reported in this paper.

Acknowledgements

The work was supported by the Portuguese Foundation for Science and Technology (FCT) through the project UID/EEA/04436/2013 and NORTE-01-0145-FEDER-000018-HAMaBICO, B-FABULUS (PTDC/BBB-ECT/2690/2014) and 3BioMed (FCT/4773/May 4, 2017/S). The F.R.M. acknowledges FCT for her contract under the Transitional Rule DL 57/2016 (CTTI-57/18-I3BS(5)). FCT/MCTES is also acknowledged for the PhD scholarship attributed to F.I.C (SFRH/BD/99555/2014) and the financial support provided to J.M.O. (IF/01285/2015) under the program "Investigador FCT".

References

Bartolomeu, F., Faria, S., Carvalho, O., Pinto, E., Alves, N., Silva, F.S., Miranda, G., 2016. Predictive models for physical and mechanical properties of Ti6Al4V produced by Selective Laser Melting. *Mater. Sci. Eng.* 663, 181–192. <https://doi.org/10.1016/j.msea.2016.03.113>.

- Bartolomeu, F., Fonseca, J., Peixinho, N., Alves, N., Gasik, M., Silva, F., Miranda, G., 2019. Predicting the output dimensions, porosity and elastic modulus of additive manufactured biomaterial structures targeting orthopedic implants. *Journal of the mechanical behavior of biomedical materials* 99, 104–117. <https://doi.org/10.1016/j.jmbbm.2019.07.023>.
- Bartolomeu, F., Dourado, N., Pereira, F., Alves, N., Miranda, G., Silva, F., 2020. Additive manufactured porous biomaterials targeting orthopedic implants: a suitable combination of mechanical, physical and topological properties. *Mater. Sci. Eng. C* 107, 110342. <https://doi.org/10.1016/j.msec.2019.110342>.
- Bohner, M., Loosli, Y., Baroud, G., Lacroix, D., 2011. Commentary: deciphering the link between architecture and biological response of a bone graft substitute. *Acta Biomater.* 7, 478–484. <https://doi.org/10.1016/j.actbio.2010.08.008>.
- Boskey, A.L., Robey, P.G., 2018. The composition of bone. Primer on the metabolic bone diseases and disorders of mineral metabolism 84–92. <https://doi.org/10.1002/9781119266594.ch11>.
- Cao, B., Li, Z., Peng, R., Ding, J., 2015. Effects of cell–cell contact and oxygen tension on chondrogenic differentiation of stem cells. *Biomaterials* 64, 21–32. <https://doi.org/10.1016/j.biomaterials.2015.06.018>.
- Denry, I., Kelly, J.R., 2008. State of the art of zirconia for dental applications. *Dent. Mater.* 24, 299–307. <https://doi.org/10.1016/j.dental.2007.05.007>.
- Garcia-Gonzalez, D., Rusinek, A., Jankowiak, T., Arias, A., 2015. Mechanical impact behavior of polyether–ether–ketone (PEEK). *Compos. Struct.* 124, 88–99. <https://doi.org/10.1016/j.compstruct.2014.12.061>.
- Gilbert, J.L., 2017. Corrosion in the human body: metallic implants in the complex body environment. *Corrosion* 73, 1478–1495. <https://doi.org/10.5006/2563>.
- Gittens, R.A., Scheideler, L., Rupp, F., Hyzy, S.L., Geis-Gerstorfer, J., Schwartz, Z., Boyan, B.D., 2014. A review on the wettability of dental implant surfaces II: biological and clinical aspects. *Acta Biomater.* 10, 2907–2918. <https://doi.org/10.1016/j.actbio.2014.03.032>.
- Giwa, S., Lewis, J.K., Alvarez, L., Langer, R., Roth, A.E., Church, G.M., Markmann, J.F., Sachs, D.H., Chandraker, A., Wertheim, J.A., 2017. The promise of organ and tissue preservation to transform medicine. *Nat. Biotechnol.* 35, 530. <https://doi.org/10.1038/nbt.3889>.
- Hallab, N.J., Bundy, K.J., O'Connor, K., Moses, R.L., Jacobs, J.J., 2001. Evaluation of metallic and polymeric biomaterial surface energy and surface roughness characteristics for directed cell adhesion. *Tissue Eng.* 7, 55–71.

- Hausser, H.-J., Brenner, R.E., 2005. Phenotypic instability of Saos-2 cells in long-term culture. *Biochem. Biophys. Res. Commun.* 333, 216–222. <https://doi.org/10.1016/j.bbrc.2005.05.097>.
- Huang, H.-H., Ho, C.-T., Lee, T.-H., Lee, T.-L., Liao, K.-K., Chen, F.-L., 2004. Effect of surface roughness of ground titanium on initial cell adhesion. *Biomol. Eng.* 21, 93–97. <https://doi.org/10.1016/j.bioeng.2004.05.001>.
- Im, G.-I., Ko, J.-Y., Lee, J.H., 2012. Chondrogenesis of adipose stem cells in a porous polymer scaffold: influence of the pore size. *Cell Transplant.* 21, 2397–2405. <https://doi.org/10.3727/096368912X638865>.
- Iqbal, N., Khan, A.S., Asif, A., Yar, M., Haycock, J.W., Rehman, I.U., 2019. Recent concepts in biodegradable polymers for tissue engineering paradigms: a critical review. *Int. Mater. Rev.* 64, 91–126. <https://doi.org/10.1080/09506608.2018.1460943>.
- Jones, A.C., Milthorpe, B., Averdunk, H., Limaye, A., Senden, T.J., Sakellariou, A., Sheppard, A.P., Sok, R.M., Knackstedt, M.A., Brandwood, A., 2004. Analysis of 3D bone ingrowth into polymer scaffolds via micro-computed tomography imaging. *Biomaterials* 25, 4947–4954. <https://doi.org/10.1016/j.biomaterials.2004.01.047>.
- Jung, H.-D., Park, H.S., Kang, M.-H., Lee, S.-M., Kim, H.-E., Estrin, Y., Koh, Y.-H., 2014. Polyetheretherketone/magnesium composite selectively coated with hydroxyapatite for enhanced in vitro bio-corrosion resistance and biocompatibility. *Mater. Lett.* 116, 20–22. <https://doi.org/10.1016/j.matlet.2013.10.062>.
- Karageorgiou, V., Kaplan, D., 2005. Porosity of 3D biomaterial scaffolds and osteogenesis. *Biomaterials* 26, 5474–5491. <https://doi.org/10.1016/j.biomaterials.2005.02.002>.
- Kuboki, Y., Takita, H., Kobayashi, D., Tsuruga, E., Inoue, M., Murata, M., Nagai, N., Dohi, Y., Ohgushi, H., 1998. BMP-induced osteogenesis on the surface of hydroxyapatite with geometrically feasible and nonfeasible structures: topology of osteogenesis. *J. Biomed. Mater. Res.* 39, 190–199. [https://doi.org/10.1002/\(SICI\)1097-4636\(199802\)39:2<190::AID-JBM4>3.0.CO;2-K](https://doi.org/10.1002/(SICI)1097-4636(199802)39:2<190::AID-JBM4>3.0.CO;2-K).
- Kubota, Y., Hayakawa, K., Okano, T., Tanaka, S., Nakamura, T., 2014. Electro-thermo-mechanical finite element analysis on DC pulse resistance pressure sintering process of zirconia part. *Procedia Engineering* 81, 2421–2426. <https://doi.org/10.1016/j.proeng.2014.10.344>.
- Leong, K., Chua, S.C., Sudarmadji, N., Yeong, W., 2008. Engineering functionally graded tissue engineering scaffolds. *Journal of the mechanical behavior of biomedical materials* 1, 140–152. <https://doi.org/10.1016/j.jmbm.2007.11.002>.
- Lu, T., Wen, J., Qian, S., Cao, H., Ning, C., Pan, X., Jiang, X., Liu, X., Chu, P.K., 2015. Enhanced osteointegration on tantalum-implanted polyetheretherketone surface with bone-like elastic modulus. *Biomaterials* 51, 173–183. <https://doi.org/10.1016/j.biomaterials.2015.02.018>.
- Mohammed, M., Babadagli, T., 2015. Wettability alteration: a comprehensive review of materials/methods and testing the selected ones on heavy-oil containing oil-wet systems. *Adv. Colloid Interface Sci.* 220, 54–77. <https://doi.org/10.1016/j.cis.2015.02.006>.
- Morelli, I., Drago, L., George, D.A., Gallazzi, E., Scarponi, S., Romanò, C.L., 2016. Masquelet technique: myth or reality? A systematic review and meta-analysis. *Injury* 47, S68–S76. [https://doi.org/10.1016/S0020-1383\(16\)30842-7](https://doi.org/10.1016/S0020-1383(16)30842-7).
- Murphy, C.M., Haugh, M.G., O'Brien, F.J., 2010. The effect of mean pore size on cell attachment, proliferation and migration in collagen-glycosaminoglycan scaffolds for bone tissue engineering. *Biomaterials* 31, 461–466. <https://doi.org/10.1016/j.biomaterials.2009.09.063>.
- Nagels, J., Stokdijk, M., Rozing, P.M., 2003. Stress shielding and bone resorption in shoulder arthroplasty. *J. Shoulder Elbow Surg.* 12, 35–39. <https://doi.org/10.1067/mse.2003.22>.
- Najeeb, S., Zafar, M.S., Khurshid, Z., Siddiqui, F., 2016. Applications of polyetheretherketone (PEEK) in oral implantology and prosthodontics. *Journal of prosthodontic research* 60, 12–19. <https://doi.org/10.1016/j.jpor.2015.10.001>.
- Navarro, M., Michiardi, A., Castano, O., Planell, J., 2008. Biomaterials in orthopaedics. *J. R. Soc. Interface* 5, 1137–1158. <https://doi.org/10.1098/rsif.2008.0151>.
- Niinomi, M., 2003. Recent research and development in titanium alloys for biomedical applications and healthcare goods. *Sci. Technol. Adv. Mater.* 4, 445. <https://doi.org/10.1016/j.stam.2003.09.002>.
- Osman, R.B., Swain, M.V., 2015. A critical review of dental implant materials with an emphasis on titanium versus zirconia. *Materials* 8, 932–958. <https://doi.org/10.3390/ma8030932>.
- Postiglione, L., Di Domenico, G., Ramaglia, L., Montagnani, S., Salzano, S., Di Meglio, F., Sbordone, L., Vitale, M., Rossi, G., 2003. Behavior of SaOS-2 cells cultured on different titanium surfaces. *J. Dent. Res.* 82, 692–696. <https://doi.org/10.1177/154405910308200907>.
- Rae, P., Brown, E., Orler, E., 2007. The mechanical properties of poly (ether-etherketone)(PEEK) with emphasis on the large compressive strain response. *Polymer* 48, 598–615. <https://doi.org/10.1016/j.polymer.2006.11.032>.
- Rasheed, T., Bilal, M., Zhao, Y., Raza, A., Shah, S.Z.H., Iqbal, H.M., 2019. Physicochemical characteristics and bone/cartilage tissue engineering potentialities of protein-based macromolecules—a review. *Int. J. Biol. Macromol.* 121, 13–22. <https://doi.org/10.1016/j.ijbiomac.2018.10.009>.
- Shard, A., Badyal, J., 1992. Surface oxidation of polyethylene, polystyrene, and PEEK: the synthon approach. *Macromolecules* 25, 2053–2054. <https://doi.org/10.1021/ma00033a034>.
- Tang, J., Peng, R., Ding, J., 2010. The regulation of stem cell differentiation by cell-cell contact on micropatterned material surfaces. *Biomaterials* 31, 2470–2476. <https://doi.org/10.1016/j.biomaterials.2009.12.006>.
- Tsunekawa, S., Asami, K., Ito, S., Yashima, M., Sugimoto, T., 2005. XPS study of the phase transition in pure zirconium oxide nanocrystallites. *Appl. Surf. Sci.* 252, 1651–1656. <https://doi.org/10.1016/j.apsusc.2005.03.183>.
- Wang, X., Xu, S., Zhou, S., Xu, W., Leary, M., Choong, P., Qian, M., Brandt, M., Xie, Y.M., 2016. Topological design and additive manufacturing of porous metals for bone scaffolds and orthopaedic implants: a review. *Biomaterials* 83, 127–141. <https://doi.org/10.1016/j.biomaterials.2016.01.012>.
- Watanabe, E., Yoshinari, M., 2016. Changes in X-ray photoelectron spectra of yttria-tetragonal zirconia polycrystal by ion sputtering. *Appl. Phys. A* 122, 339. <https://doi.org/10.1007/s00339-016-9930-0>.
- Weißmann, V., Bader, R., Hansmann, H., Laufer, N., 2016. Influence of the structural orientation on the mechanical properties of selective laser melted Ti6Al4V open-porous scaffolds. *Mater. Des.* 95, 188–197. <https://doi.org/10.1016/j.matdes.2016.01.095>.
- Wu, S., Liu, X., Yeung, K.W., Liu, C., Yang, X., 2014. Biomimetic porous scaffolds for bone tissue engineering. *Mater. Sci. Eng. R Rep.* 80, 1–36. <https://doi.org/10.1016/j.mser.2014.04.001>.
- Yang, S., Leong, K.-F., Du, Z., Chua, C.-K., 2001. The design of scaffolds for use in tissue engineering. Part I. Traditional factors. *Tissue Eng.* 7, 679–689. <https://doi.org/10.1089/107632701753337645>.
- Yang, W., Han, W., He, W., Li, J., Wang, J., Feng, H., Qian, Y., 2016. Surface topography of hydroxyapatite promotes osteogenic differentiation of human bone marrow mesenchymal stem cells. *Mater. Sci. Eng. C* 60, 45–53. <https://doi.org/10.1016/j.msec.2015.11.012>.
- Zhang, Q.-H., Cossey, A., Tong, J., 2016. Stress shielding in bone of a bone-cement interface. *Med. Eng. Phys.* 38, 423–426. <https://doi.org/10.1016/j.medengphy.2016.01.009>.